JOURNAL OF APPLIED ELECTROCHEMISTRY **27** (1997) 1355–1361

Design of dedicated instrumentation for temperature distribution measurements in solid oxide fuel cells

M. ADŽIĆ

Faculty of Mechanical Engineering, University of Belgrade, Yugoslavia

M. V. HEITOR, D. SANTOS

Instituto Superior Tecnico, Technical University of Lisbon, Portugal

Received 29 May 1996; revised 15 February 1997

A thermocouple was designed for temperature distribution measurements in solid oxide fuel cells. A theoretical model, based on mixed convective–radiative heat transfer was used to predict the thermocouple response. The proposed flat type thermocouple was shown to be a high sensitive, low error temperature sensor, capable of satisfying the requirements for solid oxide fuel cell thermal behaviour research. Thereafter, a purpose-built, thin, flat-type thermocouple has been used for temperature distribution measurements at the cathode side of a planar solid oxide fuel cell. High temperature conditions of 1223 K have been tested. Beside temperature mapping, local hot spots have been easily located.

Keywords: *solid oxide fuel cells*, *temperature distribution*, *instrumentation*

1. Introduction

Solid oxide fuel cells (SOFC) are particularly interesting because they convert primary energy into electricity and heat at efficiencies between 60% and 65% which are considerably higher than in conventional power production systems [1–4]. The environmental impact is one to two orders of magnitude lower than in conventional systems because of their very low level of pollutant emissions [1, 4].

The SOFC performance and reliability are strongly affected by the temperature at which the electrolyte plate is operated. Therefore, detailed studies on the plate surface temperature distribution is of fundamental importance for SOFC research, modelling and development.

There have been many numerical studies to predict the thermal behaviour of SOFCs [3, 5–9]. Although thermocouple probes have been used in experimental SOFC research, reports on their use are restricted only to applications for mean temperature measurements of gas flow and they are mainly used for comparison with simulation results, as reported in [10]. To the authors' knowledge, no high temperature SOFC plate surface temperature distribution research has been published.

The objective of the present work is the analysis and development of dedicated instrumentation capable of simultaneous, spatially resolved, temperature measurements at the surface and the gas temperature profile in the vicinity of the SOFC electrolyte plate.

2. Operating conditions and design requirements

A schematic diagram of the problem under consideration is shown in Fig. 1 which depicts a fuel cell in a furnace that provides the required operating temperature. The fuel cell plate surface is planar and its area is small compared to the area of the surrounding wall. The SOFC operating conditions are characterised by low velocity, high nominal temperature ($\sim$1200 K) and steady gas flows. The cell anode is subjected to the forced convective flow of fuel while the cathode is subjected to natural convective airflow. The maximum expected temperature variation of the system is $\pm$20 K around the nominal operating temperature [2, 6, 7]. It is assumed that the gases are transparent in the infrared region, therefore, the heat transfer between the cell and gases is solely by convection. It is further assumed that there is radiation heat transfer between the cell plate and the surrounding wall.

The temperature sensor design requirements are as follows. For the nominal operating temperature conditions of 1223 K the measuring sensor should enable temperature measurements with a minimum sensitivity of 0.9 K per kelvin degree of the cell plate surface temperature change. The measurement error due to the influence of radiative heat transfer from

0021-891X

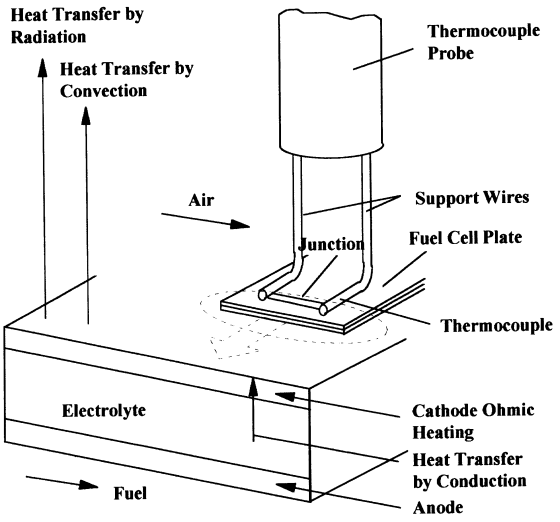

Fig. 1. Schematic of the thermocouple probe and the SOFC plate.

the surrounding wall should not exceed 0.1 K per kelvin degree of the temperature change of the surrounding wall.

3. Analysis of thermocouple response

The schematic arrangement of the thermocouple under analysis is shown in Fig. 2 which shows a flat-shaped thermocouple in the vicinity of the cell plate and parallel with it. The y coordinate axis is measured normal to the plate and its origin is on the surface of the plate. The x axis is along the axis of the thermocouple wire and its origin is defined by the centre of the thermocouple junction. It is assumed that the thermocouple surface area is small compared to both the plate surface and the chamber wall surface. The thermocouple receives heat from the plate by radiation and from the gas by convection. It loses heat to the surrounding walls by radiation and by conduction along the thermocouple wires to the support wires, as schematically shown in Fig. 2. Given these assumptions, the one-dimensional heat balance equation for the thermocouple wire, is

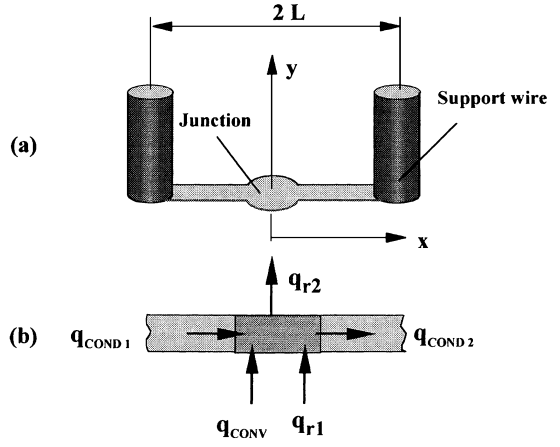

Fig. 2. (a) Schematic of the thermocouple. (b) Cross-sectional view and physical model for heat transfer.

$$\frac{\partial^2 T}{\partial x^2}+\frac{hP}{k_w A}(T_g-T)+\frac{\varepsilon\sigma P}{2k_w A}(T_1^4-T^4)-\frac{\varepsilon\sigma P}{2k_w A}(T^4-T_2^4)=\frac{\rho_w C_w}{k_w}\frac{\partial T}{\partial t} \quad (1)$$

where T, T_1, T_2 and T_g are the temperatures of the thermocouple wire, the plate surface, the surrounding wall, and the gas, respectively; k_w is the wire thermal conductivity ρ_w is the wire density and C_w is the specific heat of the wire; A is the cross-sectional area of the wire; P is the perimeter of the wire; h is the heat transfer coefficient between the surrounding gas and the wire; ε is the emissivity of the wire and σ is the Stefan–Boltzmann constant.

The temperature difference between the SOFC plate and the surrounding wall is assumed to be small enough so that T^4 may be expressed as a linear function of temperature, when expanded in Taylor's series about T_1 and T_2, thus

$$T_1^4-T^4\approx 4T_1^3(T_1-T) \quad (2)$$

and

$$T^4-T_2^4\approx 4T_2^3(T-T_2) \quad (3)$$

Substituting Equations 2 and 3 into Equation 1, and introducing the hydraulic diameter $d_h=4A/P$, the steady state heat balance equation takes the form

$$\frac{\partial^2 T}{\partial x^2}+\frac{4h}{k_w d_h}(T_g-T)+\frac{8\varepsilon\sigma}{k_w d_h}\left[T_1^4+T_2^4-T(T_1^3+T_2^3)\right]=0 \quad (4)$$

The boundary conditions are as follows:

(a) The condition of symmetry

$$\frac{\partial T}{\partial x}=0 \quad \text{at} \quad x=0 \quad (5)$$

(b) The matching condition between the thermocouple and the support wire

$$T=T_L \quad \text{at} \quad x=L \quad (6)$$

If it is further assumed that h, T_g, T_1, T_2 and d_h are given constants, the solution of Equation 4 is

$$\theta=\frac{T_g\left[1+\gamma T_*^4/(T_*^3 T_g)\right]/(1+\gamma)-T}{T_g\left[1+\gamma T_*^4/(T_*^3 T_g)\right]/(1+\gamma)-T_L}=\frac{ch(\sqrt{\alpha}x)}{ch(\sqrt{\alpha}L)} \quad (7)$$

where θ is a nondimensional temperature, while

$$T_*^3=\frac{T_1^3+T_2^3}{2} \quad (8)$$

$$T_*^4=\frac{T_1^4+T_2^4}{2} \quad (9)$$

$$\gamma=\frac{4\varepsilon\sigma T_*^3}{h} \quad (10)$$

$$\alpha=\frac{4k_g}{k_w}\frac{Nu(1+\gamma)}{d_h^2} \quad (11)$$

where γ is the radiation–convection parameter, k_g is the gas thermal conductivity and Nu is the Nusselt

number. Equation 7 gives the distribution of nondimensional temperature along the thermocouple wire. The thermocouple reading corresponds to $x = 0$, thus

$$\theta = \frac{T_g\left[1+\gamma T_*^4/(T_*^3 T_g)\right]/(1+\gamma) - T}{T_g\left[1+\gamma T_*^4/(T_*^3 T_g)\right]/(1+\gamma) - T_L} = \frac{1}{ch\left(\sqrt{\frac{4k_g}{k_w}Nu(1+\gamma)}\frac{L}{d_h}\right)} \quad (12)$$

The solution given by Equation 12 provides a means of estimating the measurement errors that may be present in the thermocouple reading, and shows the influence of the governing parameters.

To determine the range of the measurement error which may be expected in actual situations the following was assumed. The nominal operating temperature is 1223 K and $Nu = 0.5$, as suggested in [11–13]. The heat conduction contact resistance between the thermocouple and the cell plate is assumed negligible, due to the expected gas temperature gradient of the order of $\sim$1000 K m^{-1} at the plate surface. The emissivity of thermocouple wire (platinum), ε, is 0.2. Four values of the radiation convection parameter, γ, were considered and the nondimensional surface temperature $(T_1 - T)/(T_1 - T_L)$ as a function of nondimensional thermocouple length, L/d_h, is calculated, as shown in Fig. 3. The nondimensional surface temperature represents both the nondimensional measurement error and the sensitivity of the thermocouple. The curves given, in the range of $20 < L/d_h < 40$, follow one another closely, thus showing that the influence of the radiation convection parameter, γ, is negligible. The curves also indicate that the conduction errors can be further minimized by increasing L/d_h. For $L/d_h > 120$, the influence of conduction diminishes. For the limiting case where L/d_h approaches infinity the measurement error is due to the radiation and is governed solely by the radiation convection parameter, γ.

Attention will now be turned to the analysis of thermocouple support wire conduction heat transfer to provide for the boundary condition T_L. The conditions chosen are those expected during SOFC operation, namely, conditions of mixed natural convection and radiation over a horizontal surface. For the purpose of the analysis, the velocity and temperature profiles are assumed to be similar to those, for example, given in [14]. The boundary conditions are the condition of symmetry, Equa- tion 5, and the temperature T_2 at $x = L + L_1 + L_2$, where $2L$ is the thermocouple wire length; $(L_1 + L_2)$ is the length of the bare part of the support wire and L_1 is the length of the support wire parallel to the cell plate.

Equation 4 has been solved numerically for the above assumed conditions. The steady state temperature distribution along the x axis of the thermocouple is computed for two sets of values of the thermocouple wire diameter, d_h, and the surrounding temperature, T_2: (i) $d_h = 25\,\mu$m, $50\,\mu$m, $100\,\mu$m, at $T_2 = 1218$ K, and (ii) $T_2 = 1225.5$ K, 1223 K, 1218 K, for $d_h = 25\,\mu$m. The temperature distribution along the thermocouple wire is shown in Figs 4 and 5. Figure 4 clearly demonstrates the effect of the thermocouple hydraulic diameter on the difference between the actual surface temperature and the junction temperature, that is, the measurement error. The measurement error increases with the increase in wire diameter, as expected. When normalized with respect to temperature difference $(T_1 - T_2)$, the error for a $25\,\mu$m in diameter thermocouple is 5% while $100\,\mu$m in diameter thermocouple shows an error of 45%. On the other hand, it can be seen that the influence of the thermocouple wire diameter on the support wire temperature distribution is almost negligible. Thus, the temperature at the end of the thermocouple wire T_L, is practically not affected. The temperature profile of the thermocouple probe as a function of the surrounding wall temperature, T_2, is shown in Fig. 5. The curves show a pronounced influence of the surrounding wall temperature on T_L. However, the values of junction temperatures (i.e., the thermocouple readings) are substantially less affected by temperature T_2.

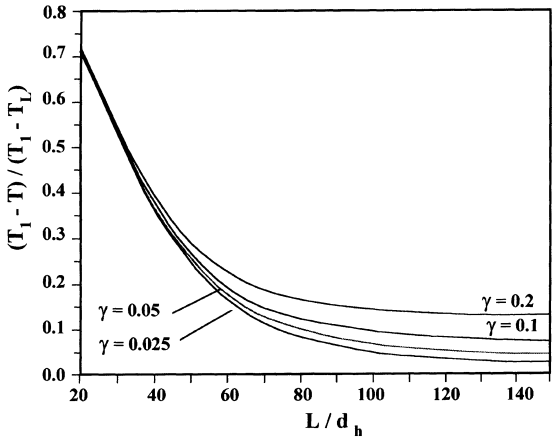

Fig. 3. Influence of the radiation convection parameter, γ, on the nondimensional surface temperature.

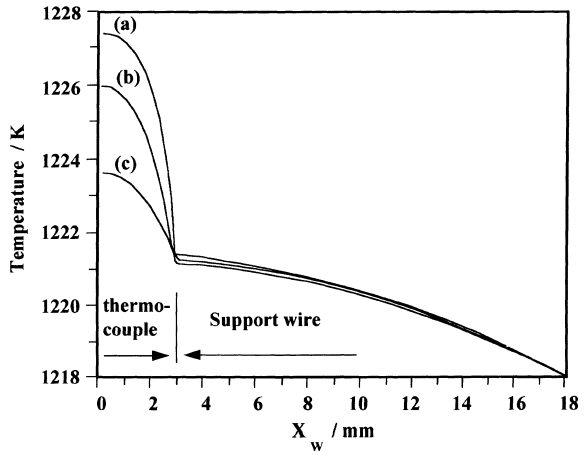

Fig. 4. Influence of the thermocouple hydraulic diameter (a) $d_h = 25\,\mu$m, (b) $d_h = 50\,\mu$m, (c) $d_h = 100\,\mu$m on the temperature distribution along the thermocouple probe for $T_1 = 1228$ K, $T_2 = 1218$ K, $\varepsilon = 0.2$.

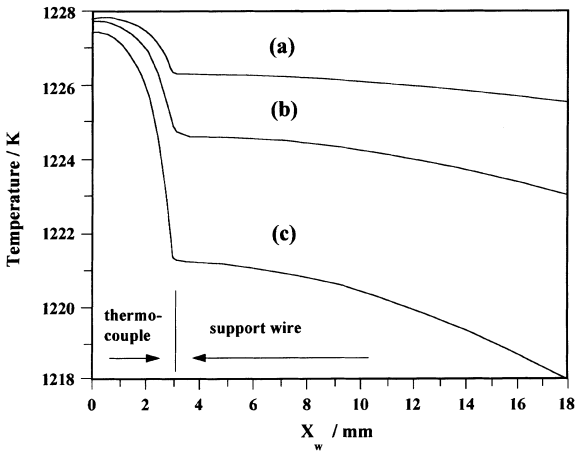

Fig. 5. Influence of the surrounding wall temperature (a) $T_2 = 1225.5$ K, (b) $T_2 = 1223$ K, (c) $T_2 = 1218$ K on the temperature distribution along the thermocouple probe for $T_1 = 1228$ K, $\epsilon = 0.2, d_h = 25\,\mu$m, $L/d_h = 120$.

The influence of the thermocouple emissivity on nondimensional air temperature in the vicinity of the cell plate (error of measurement) is shown in Fig. 6. The results are useful in estimating the measurement error due to the thermocouple emissivity and the Nusselt number. The influence of the Nusselt number is pronounced at low values of *Nu*, while at higher *Nu* values the error is mainly due to the radiative flux and the influence of *Nu* diminishes. For a platinum thermocouple and $Nu = 0.5$ the measurement error is $\pm$ 3%.

4. Instrumentation construction

Following the analysis and the measurement requirements given above, a flat type Pt–Pt/Rh13%, $d_h \approx 25\,\mu$m and $L/d_h \geq 120$ thermocouple was designed and constructed.

The approximate cross section of the sensing element was 15 μm × 80 μm. The 6 mm long thermocouple lead wires were spot welded to the 0.5 mm in diameter support wires. The support wires were insulated with a ceramic tube which was supported and protected with a refractory metal tubing.

This construction was mounted on a precision traversing mechanism which provided the desired horizontal and vertical displacement of the thermocouple, with spatial resolution of 5 μm, normal to the surface and 0.5 mm in both directions parallel with the surface.

As a thin thermocouple like this can be damaged when in contact with a solid surface, a suitable technique was developed to enable detection of the cell plate surface. Electrical potential is established between the thermocouple and the surface. A contact between the thermocouple and the plate is characterized by a sharp jump in the measured voltage. This procedure enables detection of a surface with a maximum error of 5 μm.

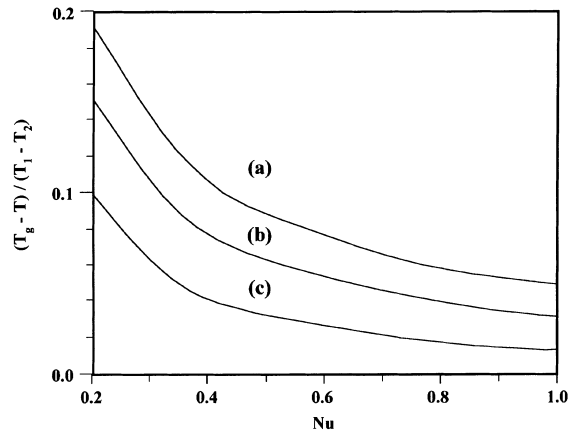

Fig. 6. Effect of the thermocouple surface emissivity (a) $\varepsilon = 0.8$, (b) $\varepsilon = 0.5$, (c) $\varepsilon = 0.2$ on the nondimensional air temperature for $d_h = 25\,\mu$m, $L/d_h = 120$.

5. Experimental setup and measurements of temperature distribution at the SOFC plate surface

Figure 7 shows a schematic diagram of the experimental facility used in this study. It consisted of a planar, solid oxide fuel cell placed inside an electrically operated and controlled furnace. The furnace chamber was 38 cm × 38 cm in cross sectional area and 45 cm in height. Three K type 0.5 mm in diameter thermocouples, flush mounted, were used for the furnace wall temperature measurements. The test rig also included a fuel supply line, exhaust gas neutralizing system, instrumentation for voltage and current measurements, instrumentation for temperature measurements, data acquisition and control system.

A 5 cm × 5 cm model SOFC of the composite flat type plate, constructed as a cosintered composite of yttria stabilized zirconia and lanthanum chromite was mounted horizontally, with the cathode facing up, in the central zone of the furnace. The plate and fuel tubings were attached to an alumina/ZrO_2 support block. The anode composed of $Ni_{0.35}(ZrO_2)_{0.65}$ was subjected to forced fuel flow, while the cathode, composed of $La_{0.84}Sr_{0.16}MnO_3$ was subjected to natural convective airflow. The Reynolds number of the fuel flow, based on the hydraulic diameter of the fuel channel, was around 10. The fuel used was 8% hydrogen in nitrogen. Both fuel and air were supplied to the fuel cell slightly above the ambient pressure. Constant fuel/air volume flow rates were maintained using electrically operated and previously calibrated flow controllers. The fuel flow rate was 620 ml min^{-1}, while the air flow rate was 1000 ml min^{-1}. The air was injected into the furnace in the downward direction, 15 cm above the cell cathode. The nominal temperature of (1223 $\pm$ 1) K was maintained constant during tests. The electric connections of the fuel cell electrodes were implemented with 0.35 mm diameter platinum wires for voltage measurements, while 0.5 mm diameter platinum wires were used for the current measurements. Both of these were welded to 50 μm thick platinum strips, which afterwards, were attached to the anode and the cathode of the fuel cell

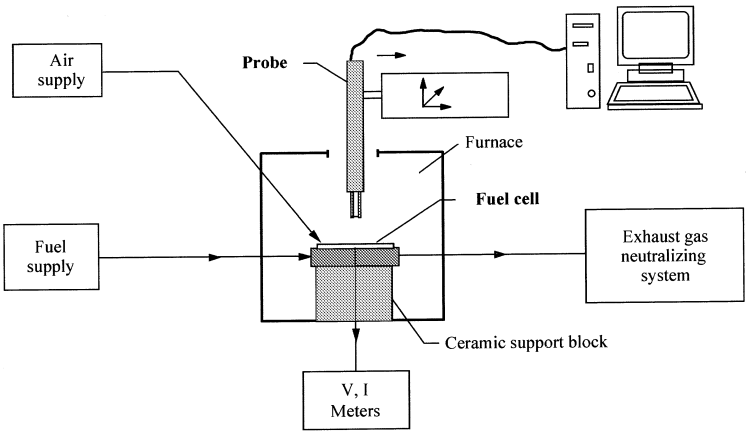

Fig. 7. Schematic diagram of the test rig.

plate, using platinum paste. To initiate the experiments, the SOFC was heated at the rate of 2 K min^{-1} upto 1223 K.

The plate surface was detected using the procedure given in the previous Section. Then, the thermocouple was lifted slightly, until there was no physical contact between the thermocouple and the plate surface. Afterwards, the thermocouple signal was amplified by a laboratory analogue amplifier, then transferred to an acquisition 12-bit board and further to a laboratory computer. At each measurement point 10 000 samples were acquired and the mean temperature was evaluated.

6. Results and discussion

The experimental results obtained refer to the cathode side of the SOFC plate. During the temperature measurements the electric cell power varied between 0.20 W and 0.28 W. The steady state behaviour of the SOFC was tested periodically during temperature measurements. It was found that the temporal variation of the temperature never exceeded 0.8 K h^{-1}.

Figure 8 shows the surface temperature distribution during a three day test cycle. The results are also presented in terms of the dimensionless temperature and the dimensionless coordinate system, as shown in Fig. 9, where the basic trends of the temperature distribution are more noticeable. In general, the region of higher temperatures correspond to higher values of X/L and Y/L, while the lower values of surface temperature are found in the region of low values of X/L and Y/L. It can also be concluded that the local hot spots and the fuel leakage areas are easily identified.

In all experiments, the maximum–minimum temperature differences measured were in the range 8–9 K. In addition, local hot spots with temperatures about 16 K above the mean surface temperature, are clearly located, as shown in Fig. 10. As expected, at the positions of the cathode–anode interconnections, at $Y/L = 0.35$ and $Y/L = 0.7$, there was a tem-

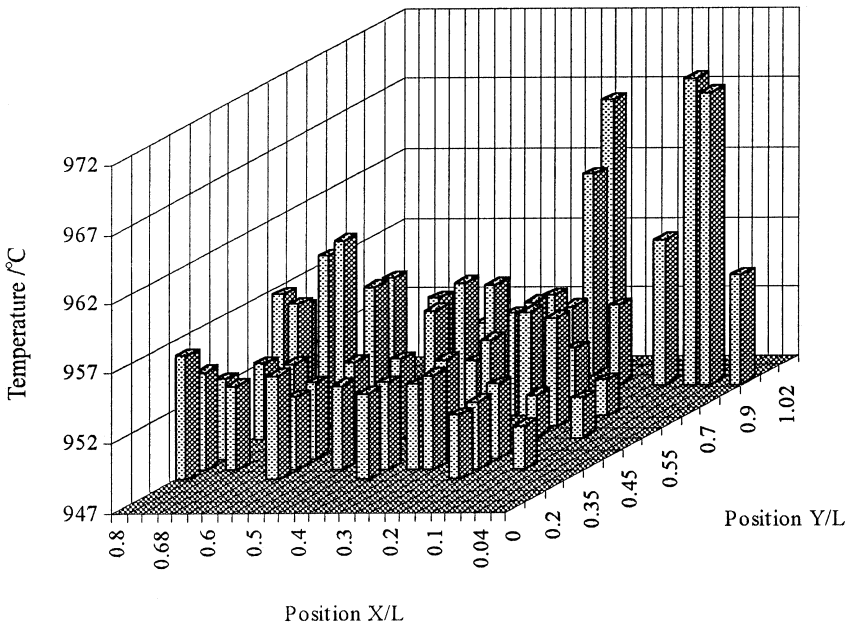

Fig. 8. Cathode surface temperature distribution.

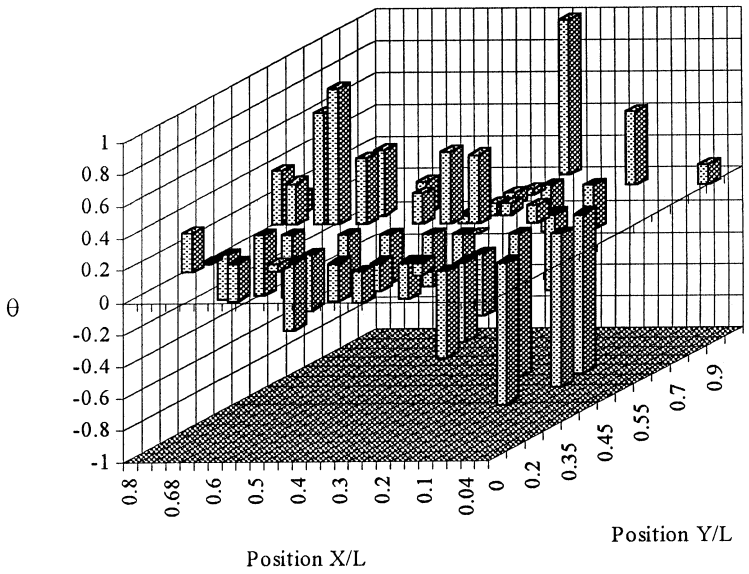

Fig. 9. Cathode surface temperature distribution. $\theta = (T_{loc} - T_{mean})\ /(T_{max} - T_{mean})$ if $T_{loc} > T_{mean}$; $\theta = (T_{loc} - T_{mean})/(T_{mean} - T_{min})$ if $T_{loc} < T_{mean}$.

perature rise in the range 3–5 K, compared to the nearby surface areas, due to increased ohmic heat production. In general, a surface temperature decrease towards the exhaust region of the fuel cell was noticed. Such behaviour can be attributed to hydrogen concentration decrease, or to fuel leakage in the region of the plate-support block contact. Figure 11 shows the temperature profile at $X/L = 0.70$ across a fuel leakage area, due to a local sealant malfunction. The area corresponds to the maximum temperature measured of 1423 K.

7. Summary

The problem of design of instrumentation for the SOFC electrolyte plate surface temperature distribution and the gas temperature profile measurements in the vicinity of a plate was studied. It is shown that the most influential parameter on the measurement error is the thermocouple length/hydraulic diameter ratio and it has been demonstrated that it is possible to keep the measurement error within reasonable limits.

Based on this analysis, it is concluded that the 25 μm in hydraulic diameter with a nondimensional length $L/d_h = 120$, thermocouple can satisfy the requirements of 0.9 K K^{-1} sensitivity. At the same time, the error of measurement, due to the radiation of the surrounding wall, is less than 0.1 K K^{-1}.

The SOFC cathode surface temperature distribution was measured using a purpose designed thin flat type thermocouple, which enabled measurements with an accuracy of ± 0.2 K.

The surface mean temperature was found to be 1226 K with local variations of ± 4 K. The anode–cathode interconnect zones showed temperatures 3–5 K higher than nearby areas. Local hot spots characterized by 16 K higher temperatures over the surface mean value were easily located. Also, a fuel leakage zone, where temperatures reached 1423 K, was found.

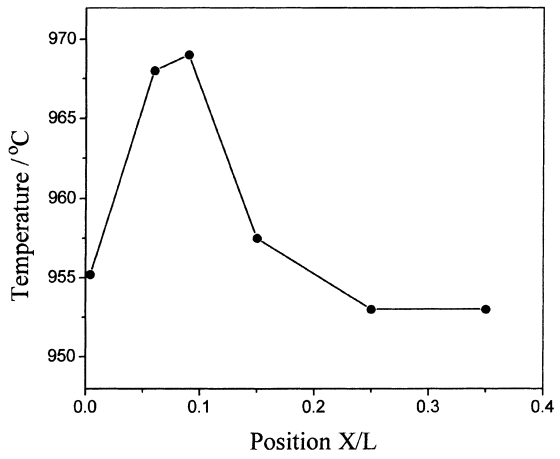

Fig. 10. Local ($Y/L = 0.9$) surface temperature indicating a hot spot.

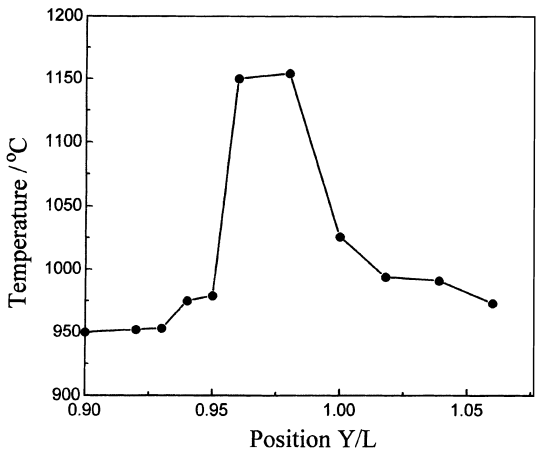

Fig. 11. Temperature profile across a fuel leakage zone.

Acknowledgements

The authors would like to express their appreciation to Dr Isabel S. de Carvalho of IST Lisbon for many helpful discussions and suggestions. Thanks are due to Sasa Damjanović of Belgrade University for his assistance in the numerical research and to Jorge Coelho of IST Lisbon for helping in the preparation of this paper. The experimental work was supported by the JOULE II Programme of the European Commission.

References

[1] 'A Ten Year Fuel Cell Research, Development and Demonstration Strategy for Europe', European Commission, December (1994).
[2] G. R. Heath and R. F. Singer, Proceedings of the Second Symposium on SOFC, Athens (1991) (edited by P. Grosz, P. Zegers, S. C. Singhal and O. Yamamoto), Office for Official Publications of the European Communities, Luxembourg, pp. 55–66.
[3] S. K. Ratkje and S. M. Holst, *Electrochim. Acta* **38** (1993) 447.
[4] M. Mogensen, *Europhys. News* **24** (1993) 7.
[5] Z. Takehara, K. Kanamura, A. Hirano and M. Ipponmatsu, Proceedings of the Second Symposium on SOFC, *op.cit* [2], pp. 313–19.
[6] E. Erdle., J. Groß, H. G. Müller, W. J. C. Müller, H.-J. Reusch, R. Sonnenschein, Proceedings of the Second Symposium on SOFC, *op.cit*. [2], pp. 265–72.
[7] J. R. Ferguson, Proceedings of the Second Symposium on SOFC, *op. cit*. [2], pp. 305–12.
[8] P. V. Hendriksen, Second Nordic Symposium on High Temperature Fuel Cells (edited by T. Norby and F. W. Poulsen), Geilo, Norway (1994), p. 16.
[9] E. Achenbach, *J. Power Sources* **49** (1994) 333.
[10] A. Hirano, M. Suzuki and M. Ipponmatsu, *J. Electrochem. Soc*. **139** (1992) 2744.
[11] J. A. B. Wills, *J. Fluid Mech*. **12** (1962) 388.
[12] V. S. Yablonski and P. P. Shumilov, 'Heat Transfer', FONTI NKTL SSSR, Moscow (1935).
[13] M. A. Miheev, 'Fundamentals of Heat Transfer', Gosenergoizdat, Moscow (1956).
[14] M. M. Ali, T. S. Chen and B. F. Armaly, *AIAA J*. **22** (1984) 1797.